*remote sensing*

MDPI

*Article*

# Early Fire Detection with Higher Sensitivity and Timeliness: Porting the RST-FIRES Algorithm to Rapid Scan Geostationary Data

**Alfredo Falconieri [1], Roberto Colonna [2], Vita Elena Di Leo [2], Carolina Filizzola [1], Giuseppe Mazzeo [1], Nicola Pergola [1,*], Carla Pietrapertosa [1] and Valerio Tramutoli [2]**

[1] Institute of Methodologies for Environmental Analysis, National Research Council, C. da S. Loja, Tito Scalo, 85050 Tito, Italy; alfredo.falconieri@cnr.it (A.F.); carolina.filizzola@cnr.it (C.F.); giuseppe-mazzeo@cnr.it (G.M.); carla.pietrapertosa@cnr.it (C.P.)

[2] Department of Engineering, University of Basilicata, Via dell'Ateneo Lucano 10, 85100 Potenza, Italy; roberto.colonna@unibas.it (R.C.); vita.dileo@unibas.it (V.E.D.L.); valerio.tramutoli@unibas.it (V.T.)

* Correspondence: nicola.pergola@cnr.it

## Highlights

### What are the main findings?

- Porting the RST-FIRES algorithm to MSG-RSS data (5-min resolution) increases fire detection sensitivity by 145% compared to the standard 15-min mode.
- The high-frequency observations significantly improve detection timeliness, providing an average lead time of 65 min before official fire reports, nearly doubling the performance of the standard configuration.

### What are the implications of the main findings?

- The proposed methodology enables the immediate operational use of RST algorithm on new satellite sensors without waiting for years of historical archives.
- These results ensure methodological continuity for the Meteosat Third Generation (MTG) mission, allowing for enhanced near-real-time monitoring and early warning systems for wildfires.

## Abstract

In this work, the portability of the Robust Satellite Techniques for FIRES detection and monitoring (RST-FIRES) has been preliminary experimented on the Spinning Enhanced Visible and InfraRed Imager (SEVIRI) aboard the Meteosat Second Generation (MSG) satellite in Rapid Scan Service (RSS) mode. Such a configuration offers 5 min of revisit time as compared with 15 min in the standard mode (0-degree). The impact in early fire detection has been assessed and quantified, also in comparison with the results of the RST-FIRES implemented on MSG/SEVIRI 0-degree data, using the official fire bulletins of the Calabria Region (Southern Italy) for the events occurred during July 2022, for which the official regional fire catalogue was available. The results obtained suggest that SEVIRI-RSS data could allow for a rather systematic earlier detection and a better sensitivity than SEVIRI 0-degree because of the improved temporal (and spatial) resolutions. These findings are remarkable in view of the next implementation of RST-FIRES on Meteosat Third Generation/Flexible Combined Imager (MTG/FCI) data, to exploit the improved spatial (2–1 km) and temporal (10–2.5 min) resolutions offered by such a new-generation

Academic Editor: Luis A. Ruiz

Received: 28 April 2026
Revised: 29 May 2026
Accepted: 4 June 2026
Published: 5 June 2026

geostationary mission, together with a more suitable dynamic range in the MIR spectral region (saturation at ~500 K @3.8 micron). The use of synthetic background reference fields would allow, in fact, for a straightforward RST-FIRES application to MTGI/FCI data allowing for a more effective fire early warning system.

**Keywords:** wildfires; early fire detection; RST-FIRES; MSG-SEVIRI; rapid scan service (RSS); MTG-FCI; change detection; thermal anomalies

## 1. Introduction

Wildfires are a worldwide phenomenon with environmental and socioeconomic impacts at global scale [1,2]. Each year, fires destroy millions of hectares of forests around the world, representing one of the major environmental emergencies, which are significantly increasing, both in number and intensity, because of climate change [3–7]. They may pose a risk for life and infrastructures, degrading air quality and perturbing large areas over a wide variety of biomes [8–11].

Many satellite-based methods for fire detection and monitoring have been developed to provide systematic and accurate information about fire locations and space-time evolutions [12]. Most of the proposed satellite methods are based on data provided by polar-orbiting platforms, like NOAA-AVHRR, EOS-MODIS and NASA-VIIRS, e.g., [13–18]. However, often the temporal frequency of these satellite products, even when merged as provided by a spurious constellation, is not adequate for an early detection and for a continuous monitoring of fire events [19].

Early detection of fires, in fact, is of paramount importance to promptly activate the countermeasures required to extinguish them before they become so intense and extensive to get out of control, increasing damages and risks to persons and properties. Moreover, fighting against smaller fires requires minor human and instrumental resources, that can be more easily and quickly activated even in remote areas. In addition, short-living events or fires characterized by very rapid evolution times requires very high observation frequency information, like the ones offered by the geostationary satellites, presently providing a quasi-continuous data flow, with refreshing times ranging from 30 min to 5 min [20–22].

Several methods have been proposed and implemented for active fire detection and monitoring by using geostationary observations [23–32]. Among those products, RST-FIRES, a multi-temporal change detection approach, has already demonstrated a significant improvement in terms of small/early-stage fire detection using EUMETSAT Meteosat Second Generation (MSG) SEVIRI (Spinning Enhanced Visible Infra-red Imager) data with temporal resolution of 15 min, despite the coarse spatial detail (i.e., ~3 km pixel size at nadir) [33]. More recently, a few studies preliminarily addressed the improved performances that new generation of geostationary systems, like the Meteosat Third Generation (MTG), are offering for detecting and characterizing active fires [34,35].

In this work, the porting of the RST-FIRES technique to the data acquired by MSG/SEVIRI in Rapid Scan Service (RSS) mode (i.e., 5-min temporal resolution) is preliminary tested and discussed, together with its implications in terms of fire detection timeliness and sensitivity, also in view of its possible application to the Meteosat Third Generation (MTG) data, offering even improved spatial detail, sampling frequency and radiometric performances [36,37]. In Section 2, the used satellite and validation datasets are described; Section 3 briefly describes the RST-FIRES technique rationale and requirements, whereas in Section 4 the issue of its porting to different sensors is discussed. Section 5 presents the methodological approach proposed for the porting procedure; achieved

results, over the selected study case are reported in Section 6. Finally, Section 7 briefly discusses the outcomes of this work whereas Section 8 outlines the future perspectives.

## 2. Data Used

### *2.1. The Meteosat Second Generation (MSG) Data Services*

The Meteosat Second Generation (MSG) program started in 2002 to improve the image quality and quantity of the First Generation (MFG) of European Geostationary satellites, allowing meteorologists to provide more accurate medium and short-term weather forecasts, and scientists to develop value-added climate- and weather-related products at improved spatial/spectral/temporal resolutions.

The MSG program is currently made up of three operational satellites, Meteosat-9, -10 and -11 in geostationary orbit (36,000 km), all of them operated by EUMETSAT (the European Organisation for the Exploitation of Meteorological Satellites). The previous platform, Meteosat-8, was retired in 2022 after nearly twenty years of service.

The 0-degree ("0deg" from now on) data service is the main mission of MSG, providing high rate SEVIRI image data over an "Earth disc" (or "full disc") including the whole Europe and Africa continents, the Atlantic Ocean, and part of the middle east geographic area (Figure 1).

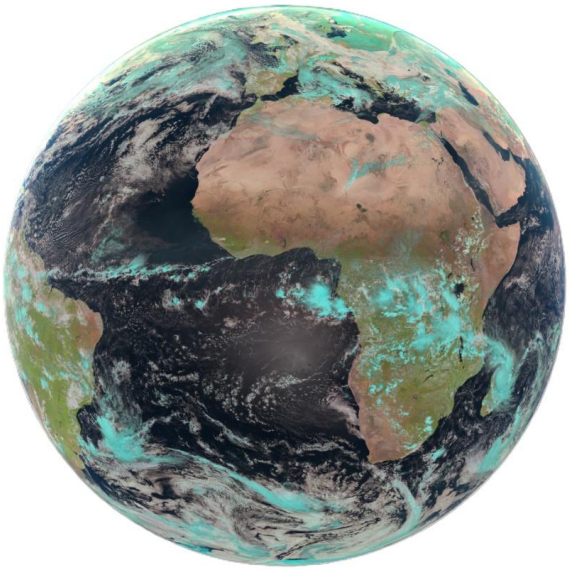

**Figure 1.** Image of the MSG 0deg full disc.

The SEVIRI instruments offer continuous observations in 12 spectral bands, scanning the full disc every 15 min. The 0deg service is presently provided by the primary Meteosat satellite (i.e., Meteosat-10), whose sub-satellite point is located at 0° Longitude [38]. Besides the latter, MSG is actually offering other services: (i) the Indian Ocean Data Coverage (IODC), delivered by Meteosat-9 satellite, positioned at 45.5°E longitude, imaging Eastern Africa and Indian ocean region every 15 min; and (ii) the Rapid Scan Service (RSS), provided by Meteosat-11 platform, which scans the northern third of the Earth disc every five minutes from a position at 9.5°E longitude, thus covering the whole European continent and north Africa (Figure 2). Both Meteosat-9 and Meteosat-11 platforms embark the same SEVIRI sensor, thus offering the same multi-spectral dataset as 0deg service.

In this work, channel 1 (centred at 0.6 μm) in the visible (VIS) range of the electromagnetic spectrum, channel 4 (centred at 3.9 μm) in the Medium InfraRed (MIR) and channel 9 (centred at 10.8 μm) in the Thermal InfraRed (TIR) have been used. All such bands have a spatial resolution of 3 × 3 km² at the sub-satellite point (nadir view).

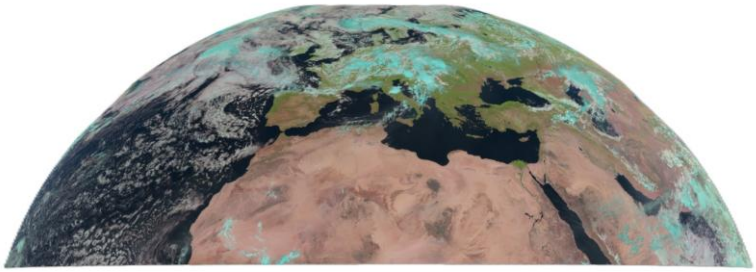

**Figure 2.** MSG RSS area coverage.

### *2.2. The Regione Calabria's Fire Catalogue*

The wildfire database used in this study, provided by the Calabria Region and obtained from the regional open data portal [39], refers to the dataset "Aree percorse da fuoco–anno 2022", which includes a census of burned areas identified through field surveys carried out by the Italian Carabinieri Forestali. The dataset belongs to the thematic area of Agriculture, is released under the Agriculture category, and is published and maintained by the Calabria Region. It was created and last updated on 2 January 2024 and is characterized by an annual updating frequency. The database includes a census of fire events that occurred within the study area during the selected period and provides, for each event, geographic coordinates, date and start time, and the burned area expressed in hectares, along with additional descriptive information such as locality, municipality, and province. The dataset also includes the classification of the event and the type of vegetation involved, allowing for a more detailed characterization of the fires. Since the event times are reported in local time, a conversion to UTC was performed to ensure temporal consistency with the satellite data used in the subsequent analyses. This conversion resulted, in some cases, in a shift of the event date to the previous day. After time normalization and quality checks, the database was considered the reference source for the localization and characterization of the wildfires occurred within the study area (i.e., Calabria Region, Southern Italy) in the considered period (i.e., July 2022) and used for validating the satellite detections. In Table 1, an extract of the fire catalogue, showing the fires officially registered in between 1–3 July, is reported.

**Table 1.** Extract from the official fire catalogue for the Calabria Region, listing fires registered between 1 and 3 July 2022. The table shows the geographic coordinates, administrative information, the date and local time registered for each fire.

| Latitude (WGS84) | Longitude (WGS84) | Municipality | Locality | Date | Time (LT) |
|---|---|---|---|---|---|
| 39.13996 | 16.827276 | Petilia Policastro | Cerasara | 1 July 2022 | 15:45 |
| 38.818592 | 16.29159 | Filadelfia | Montesoro | 1 July 2022 | 00:00 |
| 38.81798 | 16.289033 | Filadelfia | Molinello-Montesoro | 1 July 2022 | 00:00 |
| 38.644435 | 16.399462 | Cardinale | T. Usito | 2 July 2022 | 14:30 |
| 38.85877 | 16.635314 | Catanzaro | Emilia | 2 July 2022 | 10:30 |
| 39.035551 | 16.529518 | Sorbo San Basile | Capicotto | 2 July 2022 | 11:53 |
| 39.541595 | 16.188093 | Cerzeto | Serafinelli | 2 July 2022 | 14:30 |
| 39.464188 | 16.358584 | Luzzi | Fosso D'olmo | 2 July 2022 | 01:01 |
| 39.604012 | 16.052901 | Malvito | V.Ne Ritorto | 2 July 2022 | 11:43 |
| 39.565313 | 16.719308 | Paludi | Valle Del Pozzo | 2 July 2022 | 20:33 |
| 39.838754 | 15.812965 | San Nicola Arcella | Bocca Della Giarla | 2 July 2022 | 11:38 |

| | | | | | |
|---|---|---|---|---|---|
| 39.108728 | 16.117229 | San Pietro in Amantea | Conocchia-C. Pinto | 2 July 2022 | 12:00 |
| 39.020208 | 16.997243 | Cutro | Rosito | 2 July 2022 | 16:30 |
| 39.278316 | 17.014108 | Melissa | Cozzo Granatello | 2 July 2022 | 15:10 |
| 37.976457 | 16.002554 | Palizzi | Mara Giulia | 2 July 2022 | 09:53 |
| 38.453974 | 16.527843 | Stilo | Pruppa | 2 July 2022 | 14:18 |
| 38.594517 | 16.235217 | Sorianello | Collina Degli Angeli | 2 July 2022 | 07:27 |
| 39.509466 | 16.406003 | Acri | Pietremarine | 3 July 2022 | 13:40 |
| 39.506757 | 16.830413 | Mandatoriccio | Valle Napa Cipodero | 3 July 2022 | 00:00 |
| 39.258976 | 16.62818 | San Giovanni in Fiore | Ceraso | 3 July 2022 | 10:39 |
| 39.169446 | 16.913563 | Santa Severina | Valle Noce | 3 July 2022 | 12:00 |
| 39.147204 | 17.021439 | Scandale | Timpe Rosse | 3 July 2022 | 17:00 |
| 39.155336 | 17.030266 | Scandale | Corazzo | 3 July 2022 | 11:45 |
| 37.922662 | 15.956598 | Bova Marina | San Pasquale | 3 July 2022 | 13:48 |
| 38.660976 | 16.226559 | Filogaso | Torrete Brizzi | 3 July 2022 | 12:17 |

## 3. RST-FIRES: An Original Satellite-Based Technique for Early Fire Detection

The RST-FIRES algorithm is an original satellite technique, based on the more general Robust Satellite Techniques (RST) approach [40,41] and specifically designed for early fire detection. RST-FIRES identifies active fires as statistically significant thermal anomalies with respect to site-specific and time-dependent background conditions [33,42]. To this aim, specific ALICE (Absolutely Local Index of Change of the Environment) indices like [40]:

$$\otimes_V(x,y,t\ T) = \frac{V(x,y,t)-\mu_V(x,y,T)}{\sigma_V(x,y,T)} \quad (1)$$

are computed with reference to different variables V(x,y,t) each of them corresponding to cloud-free measurements made at the time t∈ T with reference to a ground resolution cell centred at the coordinates (x,y). The time domain T identifies, in our case, the collection of satellite images collected in the previous years, in the same month of the year, at the same time of the day (same time-slot); $\mu_V(x,y,T)$ and $\sigma_V(x,y,T)$ are the temporal average and the standard deviation of V(x,y,t) computed, for each position (x,y), on the collection of images identified by the time domain T.

Basically, the Brightness Temperatures (BTs) measured in the MIR and TIR bands are employed as variables V(x,y,t). For screening clouds, radiances recorded in VIS channel are also used, together with TIR signals.

Besides the standard signals usually employed in fire detection schemes (i.e., $BT_{MIR}$, $BT_{TIR}$, $\Delta BT = BT_{MIR} - BT_{TIR}$), short-term time-dependent variables (i.e., delta-slot = $BT_{MIR}$ ($t_1$) − $BT_{MIR}$ ($t_0$), where $t_1$ and $t_0$ are two consecutive time slots, 15 min apart) are also used in Equation (1) to improve sensitivity [33,43]. In Equation (1) all these variables are compared to their expected signals in unperturbed conditions (obtained by analysing long-term, multi-annual homogeneous satellite imagery identified by T) and active fires are then identified, at pixel level, as statistically significant thermal anomalies [41] depending on ALICE values. RST-FIRES, assessed and validated by means of a Total Validation Approach, carried out in collaboration with local and regional civil protection offices in three different Italian regions, has demonstrated a significant small/early-stage fire detection capability [33,43,44].

The implementation of RST-FIRES requires the availability of long-term, multi-annual and homogeneous satellite time series (at least 80 images per month in usually three–

five years, according to Koeppen et al., 2011 [45]) to construct reliable and representative background reference fields (i.e., temporal mean $\mu_V$ and standard deviation $\sigma_V$ at pixel level, respectively representing expected signal and natural variation in unperturbed conditions). This prescription may represent a critical issue when porting the algorithm to new-generation satellite sensors, such as MTG-FCI, or to different observation modes, such as the MSG-RSS, for which long-term historical datasets are still non-existent (due to the short life of the mission) or only available with a limited access (due to the huge amount of data to be downloaded and handled). In the case of MSG-RSS, the high temporal resolution (5-min repeat cycle) further amplifies this limitation, making the direct construction of background fields from RSS data highly time-consuming.

## 4. The Proposed Solution: Synthetic Background Reference Fields

To address this issue, an alternative approach was proposed and developed, consisting in the generation of synthetic RSS background reference fields derived from the already available MSG-SEVIRI 0deg reference fields, characterized by a 15-min temporal resolution. These reference datasets, built by processing about 15 years of MSG-SEVIRI 0deg time series, from 2004 to 2019, are presently available for all months, for all the spectral channels relevant to fire detection (i.e., VIS, MIR, TIR) and for all time slots (96 for a full day cycle of 24 h), ensuring consistency and completeness. This work proposes a first experimental application of this approach to RSS data, to assess its suitability for an accurate and effective porting of the RST-FIRES algorithm to higher temporal resolution observations for which there is not yet a sufficiently long history. The overall methodology was designed and implemented through a dedicated three-step processing scheme. To check the accuracy and consistency of the procedure, an actual RSS dataset (covering the region of interest, i.e., Italy area, and a specific period, i.e., June–September 2022 and 2024) has been downloaded from the EUMETSAT archive by using the EUMETSAT Data Access Client (EUMDAC, [46]) and used for comparison between synthetic and real data. September/October 2024 were used to compare synthetic and actual data from single and multiple SEVIRI RSS and MTG-FCI acquisitions (the latter of which has only been available since 24 September 2024) whereas July 2022 data were used because of the availability of the official fire bulletin.

## 5. Porting of RST-FIRES to MSG-RSS: The Methodological Approach

Before simulating the MSG-RSS background reference fields, a preliminary analysis has been carried out over single and multiple images to assess the methodological approach. The latter, was based on a three-step procedure:

Step 1: spatial resampling
Step 2: time shifting
Step 3: temporal interpolation

### *5.1. Spatial Resampling*

The same sensor (SEVIRI) is carried on board the two different Meteosat missions, i.e., Met-10 (0deg Service) and Met-11 (RSS Service). However, the platforms are located at different satellite sub-points: 0° Long for Met-10 and 9.5° Long E for Met-11. This leads to a slightly different view geometry that must be considered for a proper co-location of the two image datasets. For this purpose, an ad hoc procedure has been developed and implemented for the automatic application of a spatial resampling procedure based on the nearest neighbour (NN) approach (Figure 3) to preserve the original SEVIRI radiometric values. More in detail, our Area of Interest (Italian peninsula) is fully accommodated in a 367 × 270 pixels/lines matrix for the 0deg imagery, whereas the same area

requires a 329 × 264 matrix as far as the RSS view geometry is considered. Therefore, the NN resampling procedure was applied to the original 0deg imagery to build a resampled dataset which mimics the actual RSS data (i.e., the synthetic RSS data). One example, referring to SEVIRI MIR images of 26 September 2024 at 12:00 UTC is reported in Figure 4. The resampling procedure has been applied over Italy for the MSG-SEVIRI 0deg July reference fields, for a total of 960 spatially resampled images.

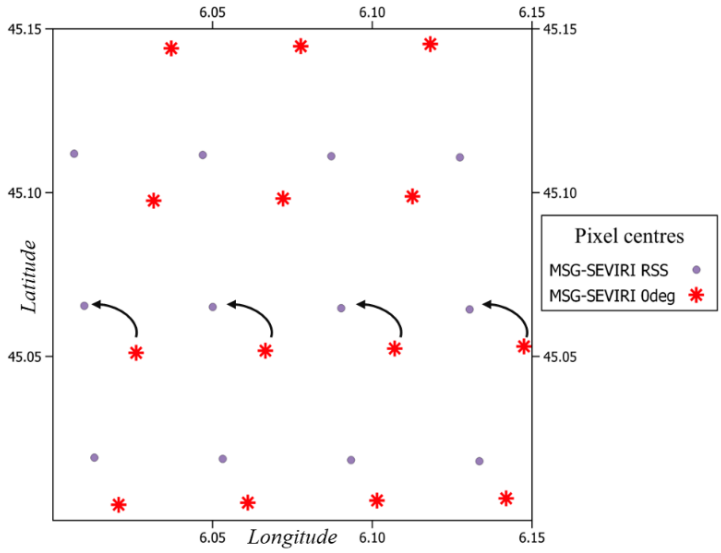


**Figure 3.** Nearest neighbour resampling scheme of 0deg to RSS grid. Red asterisks are the MSG 0deg original pixel centres coordinates, and grey dots represent the RSS pixel centre locations.

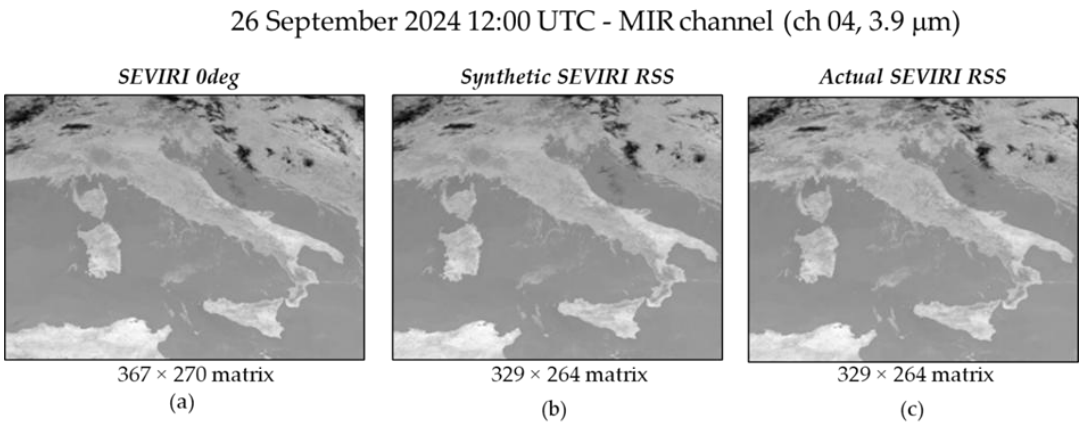


**Figure 4.** Examples of resampled versus actual images. (**a**) Original and (**b**) spatially resampled MSG 0deg images of MIR channel at 12:00 UTC on 26 September 2024; (**c**) actual MSG RSS data (acquired for the same channel, date, and time).

### *5.2. Time Shifting*

After the computation of the synthetic RSS reference fields, an analysis was performed to identify the optimal temporal correspondence between resampled MSG-SEVIRI 0deg and actual RSS observations, due to the different temporal resolutions and scanning times of the two datasets. Resampled MSG 0deg Channel 1 (Visible, VIS, centred at 0.6 μm), Channel 4 (Medium Infrared, MIR, centred at 3.9 μm), and Channel 9 (Thermal Infrared, TIR, centred at 10.8 μm) images were generated for one specific time slot and then compared with the actual RSS observations, acquired at closest times and downloaded from the EUMETSAT archive.

As an example, the synthetic RSS image of 12:00 UTC was compared to the actual RSS data acquired at 12:00, 12:05 and 12:10 UTC to assess their correlation.

As shown in Figure 5, all the analysed image pairs exhibited very high correlation values ($R^2 > 0.81$, Mean Absolute Error (MAE) < 1.45, Root Mean Square Error (RMSE) < 3.48). However, for the area of interest (Italy) and consistently across all three spectral channels, the highest correlation was found for the following temporal relationship:

MSG-SEVIRI 0deg_resampled [@HH:mm] versus MSG-RSS_actual [@HH:mm + 10].

Therefore, a 10-min shifting is systematically offering the best correlation. For example, the MSG-SEVIRI 0deg acquisition at 12:00 UTC, resampled to the RSS geometry, shows the strongest correlation (with $R^2 > 0.94$, MAE < 0.87, RMSE < 1.6) with the RSS actual acquisition at 12:10 UTC, as illustrated for the MIR, VIS and TIR channels in Figure 5.

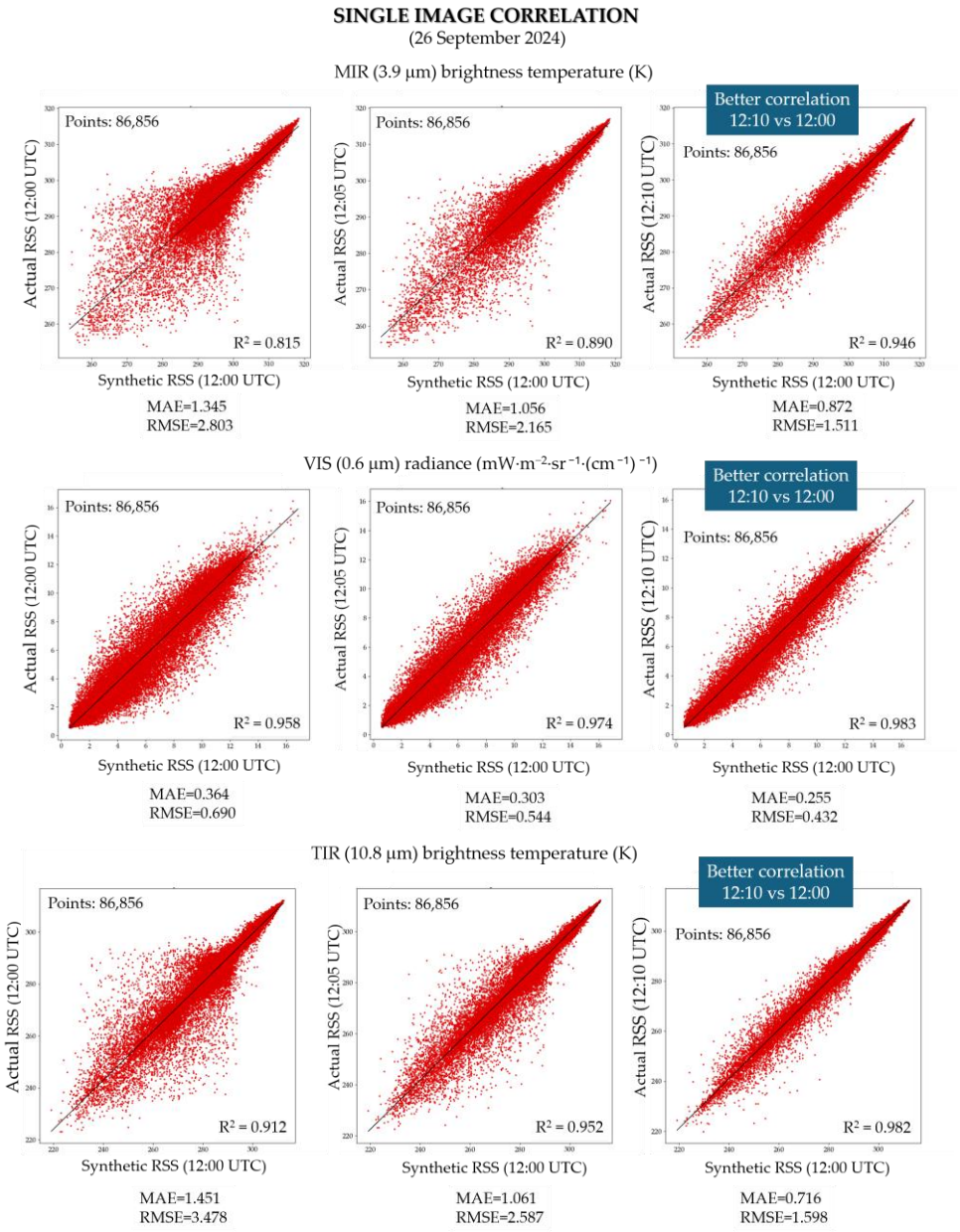


**Figure 5.** 26 September 2024: Correlation analysis between synthetic (x-axis) RSS imagery at 12:00 and actual (y-axis) RSS data acquired at 12:00 (**left panels**), 12:05 (**centre panels**) and 12:10 (**right panels**). Moving from top to bottom, results achieved for MIR (**top**), VIS (**middle**) and TIR (**bottom**) bands are shown. $R^2$, Root Mean Square Error (RMSE) and Mean Absolute Error (MAE) are reported as well.

In addition to this single-image analysis, a multi-image analysis was also conducted using all available RSS and 0deg images acquired in the month of September 2024 at 12:00 UTC, stacked all together. The results confirmed the robustness of the 10-min temporal shift, with consistently high correlation values. Figure 6 shows a representative example obtained for the TIR channel.

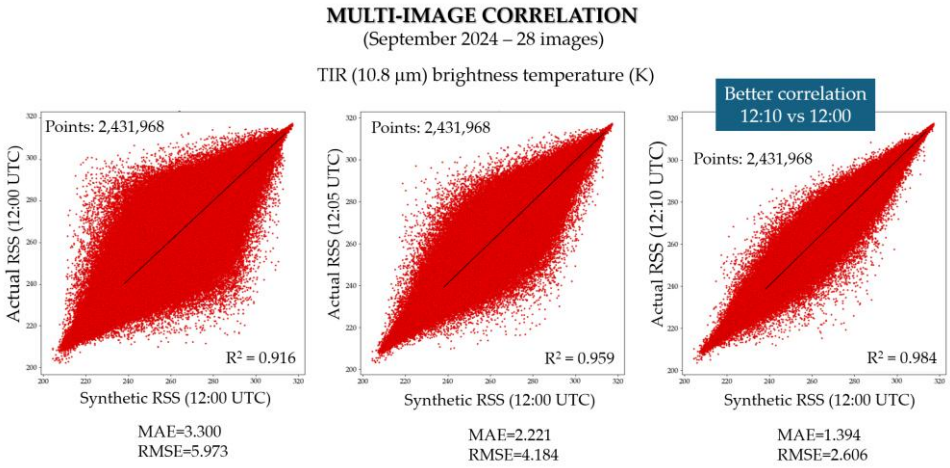


**Figure 6.** multi-image synthetic-actual RSS data correlation (TIR channel). $R^2$, MAE and RMSE are reported as well.

Such a 10-min shift, confirmed also from the analysis of all the other daily time slots, is fully expected and totally ascribable to the scanning characteristics of the RSS configuration, that is faster than 0deg in covering the (smaller) region of interest, as shown in Figure 7.

Therefore, to accurately simulate the MSG-RSS data, achieving the best possible correlation, both the spatial resampling and the 10-min shifting processes must be applied to the MSG 0deg datasets.

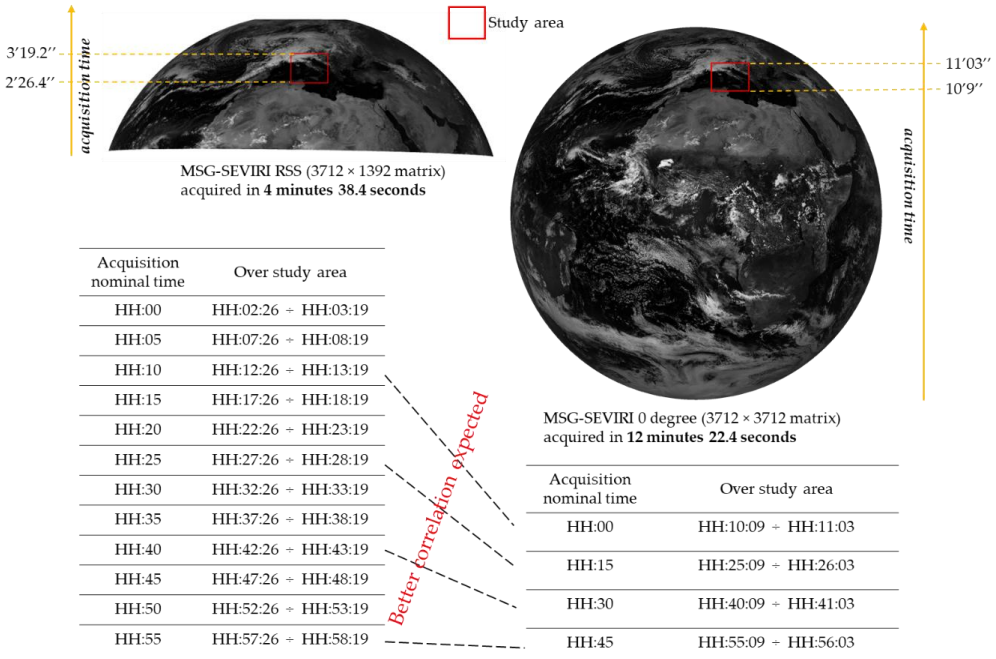


**Figure 7.** acquisition times of RSS (**left**) and 0deg (**right**) systems to reach the study area.

### *5.3. Temporal Interpolation*

Finally, to account for the different temporal resolutions of the two satellite systems, the spatially resampled images were temporally interpolated using a linear approach. Linear interpolation was selected as a conservative approximation over the 15-min interval between consecutive 0deg reference fields. Other, non-linear, interpolation methods (i.e., cubic spline) have also been tested with very similar results. The interpolation was performed according to the following relation:

$$V_t = V_{T1} + \frac{(V_{T4} - V_{T1})}{(T4 - T1)} \cdot (t\text{-}T1) \quad (2)$$

where t represents the interpolated time slot (i.e., HH:05, HH:10, HH:20, HH:25, HH:35, HH:40, HH:50, HH:55) at which the synthetic MSG-SEVIRI RSS reference fields are generated, while T1 and T4 correspond to the MSG-SEVIRI 0deg closest acquisition times (HH:00, HH:15, HH:30, HH:45) to the desired interpolated time slot (i.e., T4–T1 = 15 min). The variable $V_t$ denotes the desired, synthetic MSG-SEVIRI RSS signal value at time t, whereas $V_{T1}$ and $V_{T4}$ point out the MSG-SEVIRI 0deg signal values at times T1 and T4, respectively. Thus, for example, to obtain the interpolated value at the time slot t = HH:05, the two closest MSG-SEVIRI 0deg values, at T1 = HH:00 and T4 = HH:15 are used in equation (2). One example of the result of temporal interpolation procedure is shown in Figure 8, where the synthetic RSS reference fields (mean values) for the MIR channel in July, within the 12:00–12:15 UTC time interval are reported.

Therefore, the MSG 0deg background reference fields (n. 2, i.e., mean and standard deviation), available for all the time slots (n. 96), for all the months (n. 12), for all the variables/channels relevant for the fire detection scheme (n. 5, i.e., VIS, MIR, TIR, MIR-TIR, delta-slot) were used to calculate the synthetic MSG-RSS reference fields, according to the above described three-step procedure.

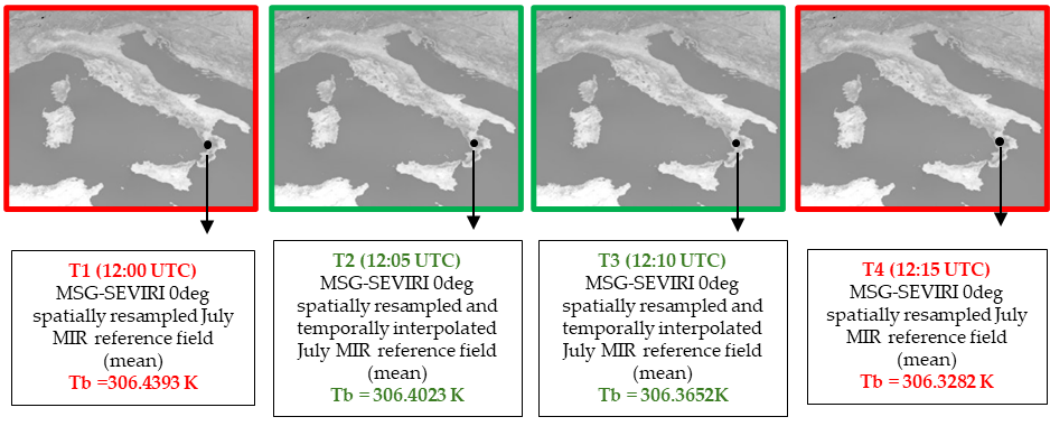


**Figure 8.** Synthetic RSS MIR mean images over 12:00–12:15 UTC temporal range. The RSS reference fields corresponding to SEVIRI 0deg time slots was obtained only by the spatial resampling (images with a red border) of the corresponding 0deg reference fields; whereas to obtain the values at higher temporal resolutions, both a spatial resampling (at the SEVIRI 0deg closest time slots) and a temporal interpolation based on Equation (2) were applied (images with a green border). Resulting BTs for one pixel of the scene (black dot, with central coordinates Lat: 39.46°N, Lon: 16.31°E) are also reported.

In Figure 9, the original MSG 0deg July refence fields (i.e., mean and standard deviation) and the synthetic RSS ones are plotted for one given pixel (Lat: 37.41°N, Long: 14:34°E) of the scene, together with the actual MIR signals observed over the same pixel on the whole day (i.e., 24 h) of 24 July 2024. The higher temporal resolution of RSS than 0deg is evident looking at the signal (red curves), whereas the actual (for 0deg) and

synthetic (for RSS) reference fields appear very similar, suggesting a smooth and reliable simulation procedure.

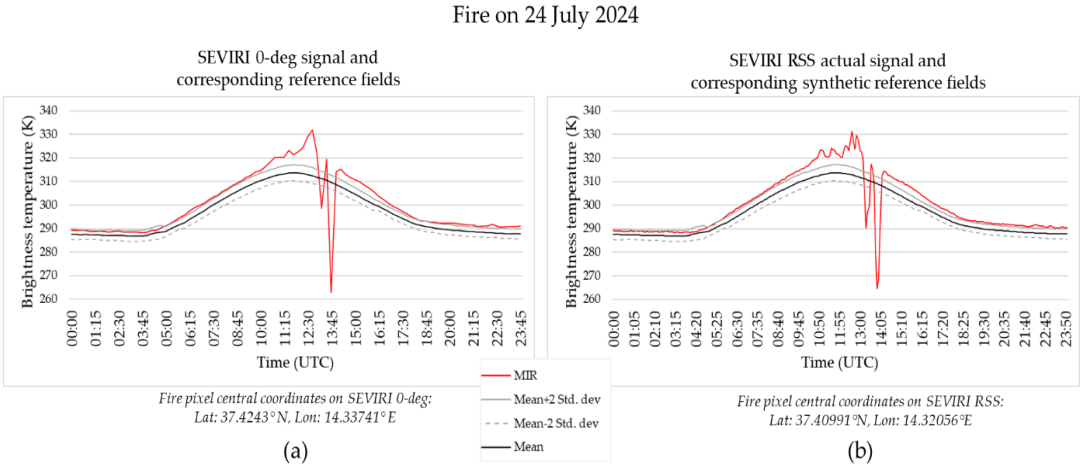


**Figure 9.** MIR signals (red line) measured at one fire pixel [37.42°N, 14.33°E] on 24 July 2024 and corresponding reference fields (mean: black line; mean ± 2 standard deviation: grey lines); (**a**) MSG-SEVIRI 0deg; (**b**) MSG-SEVIRI RSS, where the actual MIR signal is plotted together with the synthetic reference fields.

The synthetic reference fields obtained through the above-described three-step procedure have then been used to apply the RST-FIRES algorithm to RSS data over a case study and to compare the results, in terms of number of detected fires and times of detections, to the ones obtained by the same algorithm implemented on the MSG-SEVIRI 0deg dataset.

## 6. Results

The here presented experiment was carried out in the framework of the "Tech4You—Technologies for climate change adaptation and quality of life improvement" project, funded by the Next Generation EU—Italian National Recovery and Resilience Plan [47,48]. The RST-FIRES scheme has been applied to both the 0deg and RSS datasets, acquired during the month of July 2022 over the whole Calabria Region, Southern Italy. In the case of 0deg dataset, the original background reference fields have been used, together with the actual MSG-SEVIRI 0deg imagery. On the other hand, for RSS, actual SEVIRI RSS images have been employed and compared to the synthetic background reference fields, computed according to the above described 3-step procedure. The detected thermal anomalies were matched with the actual fires occurred in the region in the considered month and reported by Calabria Region's official bulletins (see Section 2.2). To this aim, a 5 km-5 h space-time buffer was adopted in the match-up analyses. Namely, the detected anomalies were considered as successfully matching an actual fire if they occur within a 5 km spatial buffer around the reported event coordinates and within a ±5 h temporal window with respect to the event time recorded in the official catalogue. The spatial selection accounts for the extent of the SEVIRI pixel size over the study area (about 5 km is the distance northwards between the centres of two adjacent pixels) and possible georeferencing errors. Therefore, it corresponds just to a 1-pixel uncertainty. About the temporal selection, the 5 h buffer was adopted as a quite restrictive option. Indeed, time delays of traditional information sources compared with the corresponding RST-FIRES identifications, even those greater than 5 h, were reported during many fire seasons [33].

Table 2 summarizes the performances, in terms of sensitivity and timeliness, of both RST-FIRES configurations over the 189 officially recorded fire events. The RSS configuration substantially improves the overall detection capability, identifying 27 events

compared to 11 fires detected using 0deg configuration, corresponding to a 145% relative increase in sensitivity.

Additionally, a slight improvement in temporal performance is also observed. The RSS configuration slightly increases the number of early detected events (from 4 to 6), but with a nearly double mean advance time, relative to the official reporting time, moving from 35 to 65 min, and extending the maximum advance time from 90 to 200 min. Therefore, the achieved results suggest for the RSS configuration a similar general capability to 0deg of detecting fires at an early stage, but a significant improvement in terms of timeliness. At the same time, the mean (maximum) delay of RSS detections increases from 89 (164) to 109 (293) minutes, showing that most of the additional RSS detections are likely delayed respect to the official fire-starting times.

**Table 2.** Detection performance (sensitivity and timeliness) of RST-FIRES applied to SEVIRI 0deg and RSS datasets in comparison with the official fire record.

| | **RST-FIRES/0deg** | **RST-FIRES/RSS** |
|---|---|---|
| Detected fires | 11 | 27 |
| Early detections | 4 | 6 |
| Delayed detections | 7 | 21 |
| Mean Advance (min) | −35 | −65 |
| Maximum Advance (min) | −90 | −200 |
| Mean delay (min) | +89 | +109 |
| Maximum delay (min) | +164 | +293 |

To further investigate the differences between the two configurations, a direct comparison focusing on the exclusive (i.e., the fires detected by one configuration only) and common (i.e., the events detected by both configurations) detections, was also performed. The results are reported in Table 3.

**Table 3.** Exclusive detection and detection timing comparison between RST-FIRES/0deg and RST-FIRES/RSS configurations.

| **SEVIRI Platform** | **Exclusive Fires** | **Common fires** | | | | |
|---|---|---|---|---|---|---|
| | | **Total Detections** | **Early Detections** | **Simultaneous Detections** | **Mean Anticipation (min)** | **Maximum Anticipation (min)** |
| RST-FIRES/0deg | 0 | 11 | 4 (vs RSS) | 2 | 37.5 (vs RSS) | 70 |
| RST-FIRES/RSS | 16 | | 5 (vs 0deg) | | 38 (vs 0deg) | 165 |

The analysis shows that the 11 fires detected using 0deg data are also identified by RSS (i.e., 0deg configuration does not allow for exclusive detections), while the latter enables the detection of additional 16 fires. Restricting the analysis to the 11 common fires, the comparison shows that, for 5 events, RSS allows for an earlier detection than 0deg, whereas 4 fires are detected by 0deg before RSS, with 2 simultaneous detections. The mean relative advance times are similar, 38 min for RSS and 37.5 min for 0deg, whereas the maximum advance observed for RSS is 165 min and 70 min for 0deg.

Regarding the sole thermal anomalies, a spatiotemporal comparison between RST-FIRES/0deg and RST-FIRES/RSS products has been accomplished. To do that, a different space-time buffer was used, namely 5 km-1 h, because no inaccuracies are expected for detection times whereas, due to the different view angles and pixel sizes, a few kilometer spatial displacement of the detected anomalies is likely to occur. The comparison revealed a significant difference in terms of total number of detections, with 134 alerts obtained from RSS data compared to 39 provided by 0deg. Therefore, the RSS detections are

roughly three times the 0deg alerts, as expected due to the triple temporal sampling offered by the Rapid Scan configuration.

Considering the 39 anomalies detected by RST-FIRES/0deg, 33 out of them (~85%) were also detected by RST-FIRES/RSS with a good consistency between the two configurations (Table 4). Regarding those 33 common anomalies, the RSS configuration provided an earlier alert than 0deg in 48.5% of the cases (16 out of 33), with an average advance of approximately 7 min. The distribution of the RSS earlier times is characterized by a median value of 5 min, indicating that most anticipations are relatively short but systematic, while there was a maximum anticipation of 30 min, highlighting the potential of RSS data to capture the early stages of fire development well in advance, under favourable conditions. Conversely, 0deg anticipates RSS in ~39% of cases (13 out of 33). Simultaneous detections account for 12.1% (4 out of 33).

From an operational perspective, the consistency of the detections with independent ground-based information further supports the reliability of the results.

Apparently, several thermal anomalies do not correlate with the fires in catalogue. However, most of them are generated by a very high (and anomalous) MIR brightness temperature and we cannot a priori exclude that they are referring to some, not documented or not reported, high temperature event (e.g., [33]).

**Table 4.** Spatiotemporal comparison between RST-FIRES/0deg and RST-FIRES/RSS thermal anomalies.

| RST-FIRES/0deg Total Anomalies | 39 | |
|---|---|---|
| 0deg exclusive occurrences | 6 | 15.4% |
| Common occurrences | *33* | *84.6%* |
| RSS earlier than 0deg | 16 | 48.5% |
| 0deg earlier than RSS | 13 | 39.4% |
| Simultaneous | 4 | 12.1% |

In Figure 10, the spatial distribution of the thermal anomalies detected by 0deg (blue) and RSS (red) RST-FIRES configurations are shown. Please note that the figure only reports the spatial dimension, i.e., the same anomaly may have been identified multiple times, at different time slots.

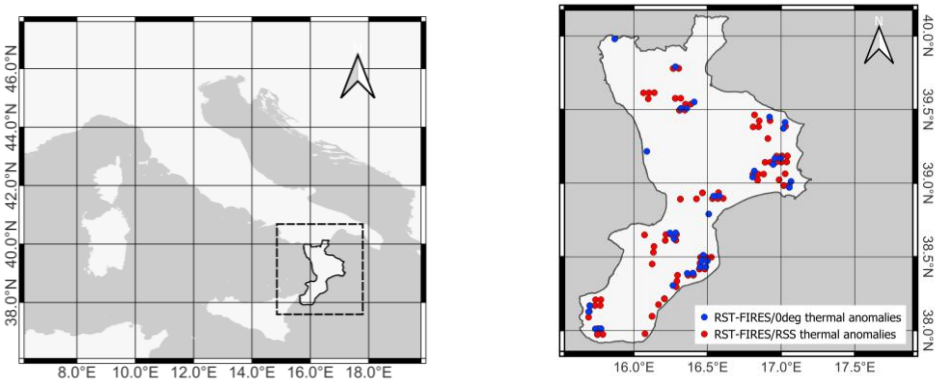


**Figure 10.** (**Left**) geographical setting of Calabria region. (**Right**) spatial distribution of the thermal anomalies detected by RST-FIRES/0deg (blue dots) and RST-FIRES/RSS (red dots).

Figure 11, reporting the MIR daily cycle signal together with the background reference fields (i.e., mean ± 2 standard deviation), shows two examples of RSS detections: one is an exclusive detection, and the other is a slight anticipation respect to 0deg warning. Considering the exclusive detection (Figure 11a), RSS was able to identify the fire at 13:05 UTC, i.e., a few minutes before the official Mandatoriccio fire time (13:13 UTC) reported

in the Regione Calabria's bulletin, representing then an effective early detection, only achievable by using RSS records. On the other hand, for what concern the Scandale fire (Figure 11b), both the RST-FIRES configurations were able to detect the event, but RSS was able to anticipate the alert 10 min sooner compared to 0deg.

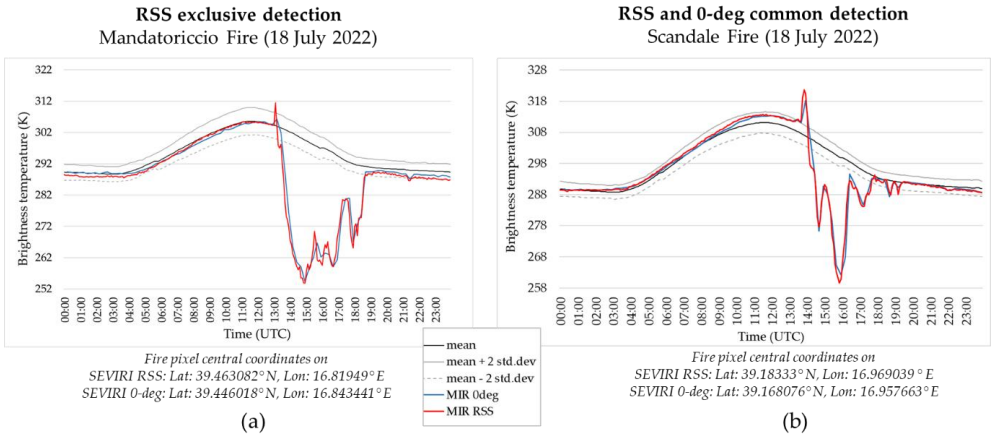


**Figure 11.** Examples of RST-FIRES/RSS exclusive (**a**) and earlier (**b**) detections compared to 0deg.

## 7. Discussion

The improvements in detection frequency and timeliness observed when using RSS data are particularly noteworthy considering that the RST-FIRES implementation at 5-min temporal resolution relies on reference fields derived through the interpolation of historical SEVIRI 0deg background statistics. Despite the lack of long-term RSS time series, which would be ideally required by the RST framework to build fully independent climatological references, the results indicate that the interpolated background fields preserve a sufficient level of physical and statistical consistency to support reliable anomaly detection at higher temporal sampling.

The significant improvement in early fire detections provided by RSS, together with the limited number of cases in which the standard configuration outperforms the rapid scan mode, suggests that the gain in temporal resolution effectively compensates for the approximations introduced in the background construction. This behavior is consistent with the underlying RST philosophy, which is designed to enhance the signal-to-noise ratio of anomalous thermal emissions by exploiting local deviations from stable reference conditions, rather than relying on absolute thresholds. In this context, the increased temporal density of observations allows for a finer tracking of the temporal evolution of fire-related thermal signals, improving the probability of intercepting the onset and early growth phases of fires.

Moreover, the increased sensitivity offered by the RSS configuration, aside from the temporal sampling, might be also ascribed to a smoothly improved spatial resolution, due to the different view geometry of RSS compared to 0deg. In fact, as previously mentioned (See Section 4), the Meteosat-11 platform providing RSS data is positioned at 9.5°E longitude, thus imaging the study area under a different (i.e., lower) view zenith angle. Looking at the study area (i.e., Calabria region), the mean zenith angles of RSS and 0deg can be computed; they are, respectively, 45.6 and 48.1 degrees, which in turn translate into a pixel area of about 12.86 and 13.48 sqkm, resulting thus in a reduction in RSS pixel size of about 5%. This means that the same fire is going to occupy a 5% greater pixel fraction in RSS imagery than 0deg, allowing for a more likely detection. This hypothesis is further corroborated by looking at the locations of the 16 additional fires exclusively detected by RST-FIRES/RSS configuration. In fact, as shown in Figure 12, most of them (12 out of 16,

i.e., 75%) are located at the easternmost area of the Calabria region, all around 17° Long E, where the 0deg view geometry is particularly unfavourable and, consequently, the improvement in terms of RSS pixel size is more enhanced. As an example, picking up the event of Crotone, occurred on 23 July 2022, located at 39.04°N and 17.03°E, the areas of the corresponding pixels are ~14.98 sqkm and ~14.07 sqkm, respectively for 0deg and RSS imagery, thus allowing effective detection by the latter because of a ~6% reduction in pixel size.

It is worth noting that the results achieved in this study are mostly independent on the spatial resampling method as well as on the interpolation function, as tests carried out by using different approaches (e.g., bilinear, cubic, spline) provided very similar results.

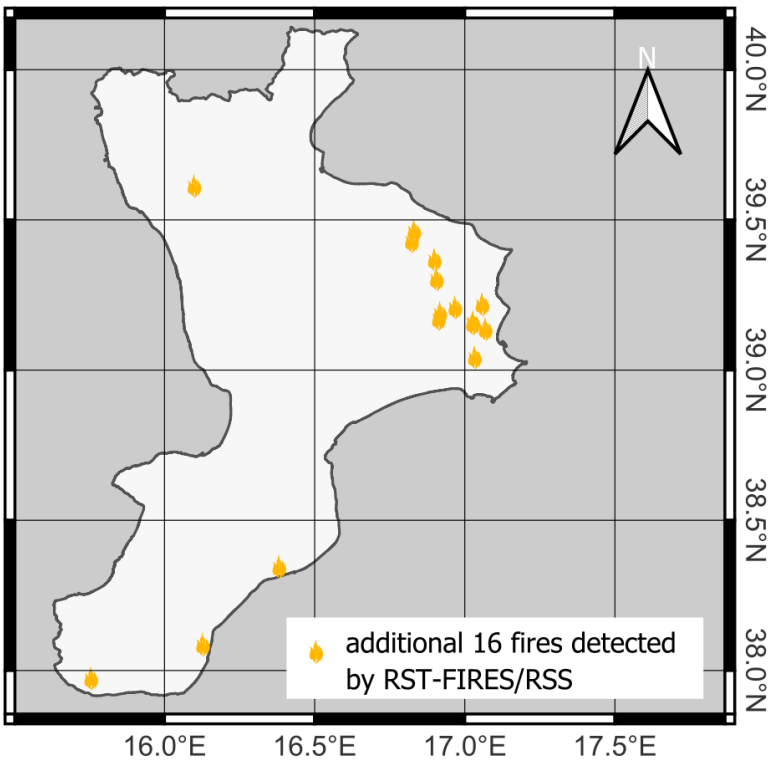


**Figure 12.** Spatial localization of the additional 16 fires detected by RST-FIRES/RSS only.

The findings of this work have relevant implications in view of the forthcoming transition to Meteosat Third Generation data [35]. The MTG-FCI instrument, in fact, is providing both enhanced spatial resolution and unprecedented temporal sampling, together with an improved dynamic range in the mid-infrared region. Furthermore, MTG-FCI is not affected by the temporary outages that characterize the RSS service, which can last from 48 h (monthly interruptions) to one month (yearly interruption).

The results presented here suggest that RST-based fire detection algorithms can effectively benefit from such improvements even when reference fields must be reconstructed or adapted from legacy datasets. With this regard, preliminary results (e.g., Figure 13) confirmed that synthetic MTG-FCI MIR imagery (@3.8 μm and 2 km of spatial resolution), obtained by resampling the MSG-SEVIRI data (@3.9 μm and 3 km) correlate very well ($R^2$ ~0.99, MAE = 0.722, RMSE = 1.412), in space-time domain, with the actual FCI data, both in night-time and daytime conditions, suggesting a smooth porting of RST-FIRES also on MTG-FCI. The latter supports the feasibility of a reliable methodological continuity between MSG-SEVIRI and MTG-FCI missions, paving the way (waiting for the latter's historical dataset to become sufficiently rich) for an immediate operational

exploitation of high-frequency and high-resolution geostationary observations for early fire detection and near-real-time monitoring.

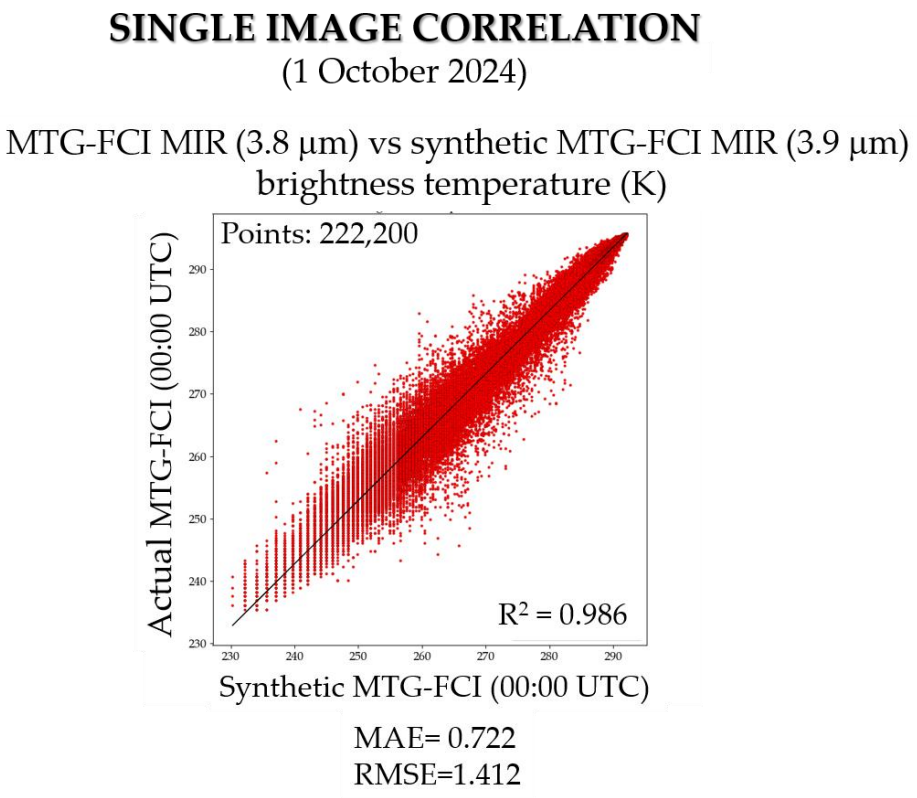


**Figure 13.** 1 October 2024: Correlation analysis between synthetic (x-axis) MTG-FCI MIR imagery and actual (y-axis) MTG-FCI MIR data acquired at 00:00 UTC. $R^2$, MAE and RMSE are reported as well.

## 8. Conclusions and Future Perspective

In this work, the porting of RST-FIRES algorithm on MSG-SEVIRI/RSS data has been preliminarily tested and assessed. Achieved results, in terms of number of fires detected and time of alerts, validated by means of an independent data set of actual fires occurred in the investigated area (Calabria Region, southern Italy) and in the considered period (July 2022), demonstrated the feasibility (and reliability) of such a porting procedure, obtained using a dataset of RSS synthetic background reference fields, derived by spatially resampling and temporally interpolating and shifting the MSG-SEVIRI 0deg data. This study demonstrated that the use of RSS data significantly improves the temporal responsiveness of RST-FIRES, allowing for a quasi-systematic earlier detection (average anticipation of 65 min, with a maximum of 200 min) than 0deg and for an increased (nearly doubled) sensitivity, due to the improved temporal (3× 0deg) and spatial (~ 5% reduction in pixel size) resolutions. Overall, these results have clear implications for near-real-time fire monitoring and early warning applications. The RST-FIRES products based on RSS data can be easily included in operational decision support tools such as the Integrated Satellite Systems (ISS, [44]). With this regard, the proposed system has been implemented over the whole Italian peninsula and operationally experimented over the Basilicata and Calabria regions in the framework of the Tech4You project. The achieved results are even more remarkable in view of the forthcoming transition to MTG data. The MTG-FCI instrument, in fact, provides both enhanced temporal sampling (10 min) and unprecedented spatial resolution (1 km) of MIR/TIR observations, together with an improved dynamic range in the mid-infrared region [49]. The results presented here suggest that RST-based fire detection algorithms can effectively benefit from such improvements even when

reference fields must be reconstructed or adapted from legacy datasets. In this reference, preliminary achievements have already demonstrated a good spatial/spectral/temporal correlation between synthetic (i.e., MSG-SEVIRI 0deg-derived) and actual MTG-FCI imagery, supporting the feasibility of a smooth operational continuity between MSG-SEVIRI and MTG-FCI missions, for early fire detection and near-real-time monitoring based on the RST-FIRES approach.

**Author Contributions:** Conceptualization, N.P. and V.T.; methodology, V.T., C.F. and A.F.; software, A.F., C.F. and C.P.; validation, A.F., V.E.D.L., R.C. and G.M.; formal analysis, A.F., C.F. and G.M.; writing—original draft preparation, A.F., G.M. and N.P.; writing—review and editing, N.P. and V.T.; funding acquisition, N.P. and V.T. All authors have read and agreed to the published version of the manuscript.

**Funding:** This research was funded by the Italian Ministry of University and Research, in the framework of the Project "TECH4YOU" (Technologies for climate change adaptation and quality of life improvement), which was funded under the National Recovery and Resilience Plan (PNRR), Mission 4–Component 2–Investment 1.5 "Innovation ecosystems", by decree of the Ministry of University and Research on 23 June 2022, project code ECS 00000009.

**Data Availability Statement:** Restrictions apply to the datasets. The datasets presented in this article are not readily available because the data are released by EUMETSAT only for Educational Use without permission for transmission or redistribution. Requests to access the datasets should be directed to EUMETSAT.

**Acknowledgments:** This research was carried out in the framework of the project "TECH4YOU" (Technologies for climate change adaptation and quality of life improvement), which was funded under the National Recovery and Resilience Plan (PNRR), Mission 4–Component 2–Investment 1.5 "Innovation ecosystems", by decree of the Ministry of University and Research on 23 June 2022, project code ECS 00000009. The authors wish to thank EUMETSAT and the Aeronautica Militare Italiana for their support in having access to the MSG/SEVIRI data used in this work.

**Conflicts of Interest:** The authors declare no conflicts of interest

## References

1. Kala, C.P. Environmental and socioeconomic impacts of forest fires: A call for multilateral cooperation and management interventions. *Nat. Hazards Res.* **2023**, *3*, 286–294. https://doi.org/10.1016/j.nhres.2023.04.003.
2. Roces-Díaz, J.V.; Santín, C.; Martínez-Vilalta, J.; Doerr, S.H. A global synthesis of fire effects on ecosystem services of forests and woodlands. *Front. Ecol. Environ.* **2022**, *20*, 170–178. https://doi.org/10.1002/fee.2349.
3. Chen, Y.; Hall, J.; van Wees, D.; Andela, N.; Hantson, S.; Giglio, L.; van der Werf, G.R.; Morton, D.C.; Randerson, J.T. Multi-decadal trends and variability in burned area from the fifth version of the Global Fire Emissions Database (GFED5). *Earth Syst. Sci. Data* **2023**, *15*, 5227–5259. https://doi.org/10.5194/essd-15-5227-2023.
4. EC-JRC. Climate Change and Wildfires, EC PSETE IV Publication. 2020. Available online: https://joint-research-centre.ec.europa.eu/system/files/2020-09/09_pesetaiv_wildfires_sc_august2020_en.pdf (accessed on 3 February 2026).
5. Flannigan, M.D.; Stocks, B.J.; Wotton, B.M. Climate change and forest fires. *Sci. Total Environ.* **2000**, *262*, 221–229. https://doi.org/10.1016/S0048-9697(00)00524-6.
6. Jones, M.W.; Abatzoglou, J.T.; Veraverbeke, S.; Andela, N.; Lasslop, G.; Forkel, M.; Smith, A.P.; Burton, C.; Betts, R.A.; van der Werf, G.R.; et al. Global and Regional Trends and Drivers of Fire Under Climate Change. *Rev. Geophys.* **2022**, *60*, e2020RG000726. https://doi.org/10.1029/2020RG000726.
7. OECD—Organisation for Economic Co-operation and Development. *Taming Wildfires in the Context of Climate Change, Report*; OECD Publishing: Paris, France, 2023. https://doi.org/10.1787/dd00c367-en.
8. Duff, T.J.; Penman, T.D. Determining the likelihood of asset destruction during wildfires: Modelling house destruction with fire simulator outputs and local-scale landscape properties. *Saf. Sci.* **2021**, *139*, 105196. https://doi.org/10.1016/j.ssci.2021.105196.

9. Jhariya, M.K.; Raj, A.K. Effects of wildfires on flora, fauna and physico-chemical properties of soil—An overview. *J. Appl. Nat. Sci.* **2014**, *6*, 887–897. https://doi.org/10.31018/jans.v6i2.550.
10. Roberts, R.; Wooster, M.J. Global impact of landscape fire emissions on surface level PM2.5 concentrations, air quality exposure and population mortality. *Atmos. Environ.* **2021**, *252*, 118210. https://doi.org/10.1016/j.atmosenv.2021.118210.
11. Zhang, T.; Wooster, M.J.; de Jong, M.C.; Xu, W. How well does the 'small fire boost' methodology used within the GFED4.1s fire emissions database represent the timing, location and magnitude of agricultural burning? *Remote Sens.* **2018**, *10*, 823. https://doi.org/10.3390/rs10060823.
12. Wooster, M.; Roberts, G.; Giglio, L.; Roy, D.; Freeborn, P.; Boschetti, L.; Justice, C.; Ichoku, C.; Schroeder, W.; Davies, D.; et al. Satellite remote sensing of active fires: History and current status, applications and future requirements. *Remote Sens. Environ.* **2021**, *267*, 112694. https://doi.org/10.1016/j.rse.2021.112694.
13. Csiszar, I.; Schroeder, W.; Giglio, L.; Ellicott, E.; Vadrevu, K.P.; Justice, C.O.; Wind, B. Active fires from the Suomi NPP visible infrared imaging radiometer suite: Product status and first evaluation results. *J. Geophys. Res. Atmos.* **2014**, *119*, 803–816. https://doi.org/10.1002/2013JD020453.
14. Giglio, L.; Kendall, J.D.; Justice, C.O. Evaluation of global fire detection algorithms using simulated AVHRR infrared data. *Int. J. Remote Sens.* **1999**, *20*, 1947–1985. https://doi.org/10.1080/014311699212290.
15. Giglio, L.; Descloitres, J.; Justice, C.O.; Kaufman, Y. An enhanced contextual fire detection algorithm for MODIS. *Remote Sens. Environ.* **2003**, *87*, 273–282. https://doi.org/10.1016/S0034-4257(03)00184-6.
16. Kaufman, Y.J.; Justice, C.O.; Flynn, L.P.; Kendall, J.D.; Prins, E.M.; Giglio, L.; Ward, D.E.; Menzel, W.P.; Setzer, A.W. Potential global fire monitoring from EOS-MODIS. *J. Geophys. Res.-Atmos.* **1998**, *103*, 32215–32238. https://doi.org/10.1029/98JD01644.
17. Schroeder, W.; Oliva, P.; Giglio, L.; Csiszar, I. The new VIIRS 375 m active fire detection data product: Algorithm description and initial assessment. *Remote Sens. Environ.* **2014**, *143*, 85–96. https://doi.org/10.1016/j.rse.2013.12.008.
18. Wooster, M.J.; Xu, W.; Nightingale, T. Sentinel-3 SLSTR active fire detection and FRP product: Pre-launch algorithm development and performance evaluation using MODIS and ASTER datasets. *Remote Sens. Environ.* **2012**, *120*, 236–254. https://doi.org/10.1016/j.rse.2011.09.033.
19. Laneve, G.; Cadau, E.G.; Castronuovo, M.M. Assessment of the fire detection limit using SEVIRI/MSG sensor. In Proceedings of the IEEE International Conference on Geoscience and Remote Sensing Symposium (IGARSS), Denver, CO, USA, 31 July–4 August 2006; pp. 4157–4160. https://doi.org/10.1109/IGARSS.2006.1066.
20. Bessho, K.; Date, K.; Hayashi, M.; Ikeda, A.; Imai, T.; Inoue, H.; Kumagai, Y.; Miyakawa, T.; Murata, H.; Ohno, T.; et al. An Introduction to Himawari-8/9—Japan's New-Generation Geostationary Meteorological Satellites. *J. Meteorol. Soc. Jpn.* **2016**, *94*, 151−183. https://doi.org/10.2151/jmsj.2016-009.
21. Krimchansky, A.; Machi, D.; Cauffman, S.A.; Davis, M.A. Next-generation Geostationary Operational Environmental Satellite (GOES-R series): A space segment overview. In *Sensors, Systems, and Next-Generation Satellites VIII*; SPIE: Bellingham, WA, USA; Volume 5570. https://doi.org/10.1117/12.565281.
22. Schmetz, J.; Pili, P.; Tjemkes, S.; Just, D.; Kerkmann, J.; Rota, S.; Ratier, A. An Introduction To Meteosat Second Generation (MSG). *Bull. Am. Meteor. Soc.* **2002**, *83*, 977–992. https://doi.org/10.1175/1520-0477(2002)083<0977:AITMSG>2.3.CO;2.
23. Hall, J.V.; Schroeder, W.; Rishmawi, K.; Wooster, M.; Schmidt, C.C.; Huang, C.; Csiszar, I.; Giglio, L. Geostationary active fire products validation: GOES-17 ABI, GOES-16 ABI, and Himawari AHI. *Int. J. Remote Sens.* **2023**, *44*, 3174–3193. https://doi.org/10.1080/01431161.2023.2217983.
24. Koltunov, A.; Ustin, S.L.; Prins, E.M. On timeliness and accuracy of wildfire detection by the GOES WF-ABBA algorithm over California during the 2006 fire season. *Remote Sens. Environ.* **2012**, *127*, 194–209. https://doi.org/10.1016/j.rse.2012.09.001.
25. Laneve, G.; Castronuovo, M.M.; Cadau, E.G. Continuous monitoring of forest fires in the Mediterranean area using MSG. *IEEE Trans. Geosci. Remote Sens.* **2006**, *44*, 2761–2768. https://doi.org/10.1109/TGRS.2006.881716.
26. Prins, E.M.; Menzel, W.P. Geostationary satellite detection of biomass burning in South America. *Int. J. Remote Sens.* **1992**, *13*, 2783–2799. https://doi.org/10.1080/01431169208904081.
27. Roberts, G.J.; Wooster, M.J. Fire detection and fire characterization over Africa using Meteosat SEVIRI. *IEEE Trans. Geosci. Remote Sens.* **2008**, *46*, 1200–1218. https://doi.org/10.1109/TGRS.2008.915751.
28. Wooster, M.J.; Roberts, G.; Freeborn, P.H.; Xu, W.; Govaerts, Y.; Beeby, R.; He, J.; Lattanzio, A.; Fisher, D.; Mullen, R. LSA SAF Meteosat FRP products—Part 1: Algorithms, product contents and analysis. *Atmos. Chem. Phys.* **2015**, *15*, 13217–13239. https://doi.org/10.5194/acp-15-13217-2015.

29. Xu, W.; Wooster, M.J.; Roberts, G.; Freeborn, P. New GOES imager algorithms for cloud and active fire detection and fire radiative power assessment across North, South and Central America. *Remote Sens. Environ.* **2010**, *114*, 1876–1895. https://doi.org/10.1016/j.rse.2010.03.012.
30. Xu, W.; Wooster, M.J.; Kaneko, T.; He, J.P.; Zhang, T.R.; Fisher, D. Major advances in geostationary fire radiative power (FRP) retrieval over Asia and Australia stemming from use of Himarawi-8 AHI. *Remote Sens. Environ.* **2017**, *193*, 138–149. https://doi.org/10.1016/j.rse.2017.02.024.
31. Xu, W.; Wooster, M.J.; He, J.; Zhang, T. Improvements in high-temporal resolution active fire detection and FRP retrieval over the Americas using GOES-16 ABI with the geostationary fire thermal anomaly (FTA) algorithm. *Sci. Remote Sens.* **2021**, *3*, 100016. https://doi.org/10.1016/j.srs.2021.100016.
32. Zhang, S.; Xue, Y.; Ling, X.; Wu, C.; Han, L.; Li, Z. Research on forest and grassland fire detection algorithm based on Himawari-8 geostationary satellite. *Int. J. Remote Sens.* **2026**, *47*, 3023–3043. https://doi.org/10.1080/01431161.2026.2625520.
33. Filizzola, C.; Corrado, R.; Marchese, F.; Mazzeo, G.; Paciello, R.; Pergola, N.; Tramutoli, V. RST-FIRES, an exportable algorithm for early-fire detection and monitoring: Description, implementation, and field validation in the case of the MSG-SEVIRI sensor. *Remote Sens. Environ.* **2017**, *192*, e2–e25. https://doi.org/10.1016/j.rse.2017.01.019.
34. Pampanoni, V.; Laneve, G.; Saquella, S.; Ferrari, A. The Fire Detection Capabilities of Meteosat Third Generation: A Comparison with Meteosat Second Generation Using Early Operational Data. In Proceedings of the IGARSS—2025 IEEE International Geoscience and Remote Sensing Symposium, Brisbane, Australia, 3–8 August 2025; pp. 3121–3125. https://doi.org/10.1109/IGARSS55030.2025.11242795.
35. Xu, W.; Wooster, M.J.; He, J.; Meraner, A.; Gomez-Dans, J.; Liu, Z.; Trigo, I.F.; Dutra, E. Major improvements in spaceborne early fire detection and small-fire FRP retrieval with the Meteosat Third Generation Flexible Combined Imager. *Sci. Remote Sens.* **2026**, *13*, 100366. https://doi.org/10.1016/j.srs.2026.100366.
36. Holmlund, K.; Grandell, J.; Schmetz, J.; Stuhlmann, R.; Bojkov, B.; Munro, R.; Lekouara, M.; Coppens, D.; Viticchie, B.; August, T.; et al. Meteosat third generation (MTG): Continuation and innovation of observations from geostationary orbit. *Bull. Am. Meteorol. Soc.* **2021**, *102*, E990–E1015. https://doi.org/10.1175/BAMS-D-19-0304.1.
37. Remoué, N.; Chetrite, B.; Bordot, G.; Martin, P.; Aminou, D.; Miranda, M.; Wilson, M. Meteosat Third Generation: MTG-I FCI PFM instrument radiometric performance. In *International Conference on Space Optics—ICSO 2022*; SPIE: Bellingham, Washington, USA, 2022; Volume 12777. https://doi.org/10.1117/12.2689288.
38. EUMETSAT, 2026—MSG 0-Degree Service. Available online: https://user.eumetsat.int/data/satellites/meteosat-second-generation/0-degree-service (accessed on 4 February 2026).
39. Open Data Calabria—Aree Percorse da Fuoco Anno 2022. 2024. Available online: https://dati.regione.calabria.it/catalogo/e2b70f8d-be0e-48c2-8dad-1ff2b1454150 (accessed on 3 February 2026).
40. Tramutoli, V. Robust AVHRR techniques (RAT) for environmental monitoring: Theory and applications, earth surface remote sensing. In *Earth Surface Remote Sensing II*; SPIE: Bellingham, WA, USA, 1998; Volume 3496, pp. 101–113. https://doi.org/10.1117/12.332714.
41. Tramutoli, V. Robust Satellite Techniques (RST) for Natural and Environmental Hazards Monitoring and Mitigation: Theory and Applications. In Proceedings of the 2007 International Workshop on the Analysis of Multi-Temporal Remote Sensing Images, Leuven, Belgium, 18–20 July 2007; pp. 1–6. https://doi.org/10.1109/MULTITEMP.2007.4293057.
42. Filizzola, C.; Falconieri, A.; Lacava, T.; Marchese, F.; Masiello, G.; Mazzeo, G.; Pergola, N.; Pietrapertosa, C.; Serio, C.; Tramutoli, V. Fire Characterization by Using an Original RST-Based Approach for Fire Radiative Power (FRP) Computation. *Fire* **2023**, *6*, 48. https://doi.org/10.3390/fire6020048.
43. Mazzeo, G.; Marchese, F.; Filizzola, C.; Pergola, N.; Tramutoli, V. A Multi-Temporal Robust Satellite Technique (RST) for Forest Fire Detection. In Proceedings of the 2007 International Workshop on the Analysis of Multi-Temporal Remote Sensing Images, Leuven, Belgium, 18–20 July 2007. https://doi.org/10.1109/MULTITEMP.2007.4293060.
44. Mazzeo, G.; De Santis, F.; Falconieri, A.; Filizzola, C.; Lacava, T.; Lanorte, A.; Marchese, F.; Nolè, G.; Pergola, N.; Pietrapertosa, C.; et al. Integrated Satellite System for Fire Detection and Prioritization. *Remote Sens.* **2022**, *14*, 335. https://doi.org/10.3390/rs14020335.
45. Koeppen, W.; Pilger, E.; Wright, R. Time series analysis of low resolution thermal infrared satellite data for detecting thermal anomalies: A hybrid approach. *Bull. Volcanol.* **2011**, *73*, 577–593. https://doi.org/10.1007/s00445-010-0427-y.
46. EUMDAC, 2025—EUMETSAT Data Access Client (EUMDAC) Guide. Available online: https://user.eumetsat.int/resources/user-guides/eumetsat-data-access-client-eumdac-guide#ID-Search-products (accessed on 2 February 2026).

47. NRRP—National Recovery and Resilience Plan. 2021. Available online: https://www.mef.gov.it/en/focus/The-National-Recovery-and-Resilience-Plan-NRRP/ (accessed on 3 February 2026).
48. TECH4YOU—Technologies for Climate Change Adaptation and Quality of Life Improvement. 2022. Available online: https://www.mur.gov.it/sites/default/files/2022-06/22_06_28%20Scheda_ecosistema_Calabria_PNRR_MUR.pdf (accessed on 5 February 2026).
49. Filizzola, C.; Mazzeo, G.; Marchese, F.; Pietrapertosa, C.; Pergola, N. The Contribution of Meteosat Third Generation–Flexible Combined Imager (MTG-FCI) Observations to the Monitoring of Thermal Volcanic Activity: The Mount Etna (Italy) February–March 2025 Eruption. *Remote Sens.* **2025**, *17*, 2102. https://doi.org/10.3390/rs17122102.